Robotica (2006) volume 24, pp. 239–250. © 2005 Cambridge University Press
doi:10.1017/S0263574705002079 Printed in the United Kingdom

Optimal kinematic design of a three translational DoFs parallel manipulator

Xin-Jun Liu

Manufacturing Engineering Institute, Department of Precision Instruments, Tsinghua University, Beijing, 100084 (P. R. of China). E-mail: xinjunl@yahoo.com

(Received in Final Form: May 6, 2005, first published online 17 November 2005)

SUMMARY

In this paper, an optimal kinematic design method of a three translational DoFs parallel manipulator is presented. The design is based on the concept of performance chart, which can show the relationship between a criterion and design parameters graphically and globally. The normalization on the design parameters of the studied manipulator makes it possible that the design space, which is made up of the normalized parameters, is limited. The design space includes of all possible *basic similarity manipulators* (BSMs). As any one of the BSMs represents all of its *similarity manipulators* (SMs) in terms of performances, if one BSM is optimal, its SMs are optimized as well. The said optimal BSM is from the optimum region, which is the intersecting result of involved performance charts. In this paper, the related performance criteria are *good-conditioning workspace* (GCW), *global conditioning index* (GCI) and *global stiffness index* (GSI). As an applying example, a design result of the parallel manipulator with a desired task workspace is presented. The results of the paper are very useful for the design and application of a parallel manipulator.

KEYWORDS: Optimum design; Parallel manipulators; Design space; Singularity.

I. INTRODUCTION

In the past two decades, parallel manipulators have attracted more and more researchers' attention in terms of industrial applications, especially in the field of machine tools, due to their relative advantages, e.g., high stiffness, high accuracy, low moving inertia, and so on. For such reasons, more and more parallel manipulators with specified number and type of degree of freedom (DoF) have been proposed. Especially, parallel manipulators with less than 6 DoFs are becoming increasingly popular in the machine tool industry.

In the family of 3-DoF parallel manipulators, the manipulators with three translational DoFs are attractive. As most industrial applications need the translations along three normal axes, such parallel manipulators have been studied and used extensively. There is no doubt that the DELTA robot[1] and its topologies are the most successful parallel manipulator designs. The DELTA robot is such a parallel manipulator that is built using spatial parallelogram mechanisms. The robot came up firstly at 1986 by means of a WIPO patent.[2] Since then, many studies have been contributed to the kinematics, dynamics and design of the DELTA robot and its topology architectures.[3–12]

It is worth mentioning that there is another parallel manipulator with three translational DoFs proposed by Tsai and Stamper,[13] which consists of only revolute joints and is made up of planar parallelograms. Without multi-DoF joints in it, the parallel manipulator has larger workspace than the DELTA robot. Both Tsai's manipulator and DELTA robot with linear actuators can be applied in the field of machine tools. Although, some papers (see Refs. [8,14]) have addressed the optimal design of the manipulators, it is necessary to develop a multi-criterion design method that can be more precise and effective. This paper addresses the optimum design of the Tsai's manipulator with linear actuators.

A parallel manipulator is such a system that the moving platform is connected to the base by at least two legs, which leads to complex kinematics and interference between legs. For such reasons, parallel manipulators have the disadvantages in terms of relatively small useful workspace. Workspace is one of the most important issues because it determines the region where the manipulator can reach. The workspace is, therefore, the most important index to design a manipulator.[15–17]

For the issue of optimal design of parallel manipulators, most methods are first to develop an objective function and then to reach the result using the numerical method with an algorithm.[9,15–18] These methodologies have the disadvantages in common, i.e. the objective function is highly non-linear and the process is iterative and time consuming. These methods can provide an optimal result. But, the consumer cannot know how optimal the result is; at least, they did not give us any proof about it. One of the most convictive designs is maybe that achieved from comparison. This method needs the tool of performance chart, which is widely used in the classical design and most design manuals. A manipulator usually has several design parameters, and each of them, especially link lengths, can have any value between zero and infinite. In order to present the performance chart in a finite space, it is necessary to normalize the involved design parameters. There are two approaches about the parameter normalization. One is that dividing all parameters by one of them.[19] However, this kind of normalization cannot make sure that the normalized

parameters are finite. Thus, the developed design space cannot be used to plot performance charts. Another one is that dividing all parameters by their average,[11,20,21] which is referred to as the normalization factor. This normalization makes sure that not only the normalized parameters are finite but the sum of all parameters is constant as well. This is very useful for the representation of a performance chart and the performance comparison of different manipulators. This paper extends the concept to the design of the three translational DoFs parallel manipulator. The analysis in this paper will show that the normalization factor doesn't change the similarity of manipulators' performances. This is the most important point in the kinematic design.

Generally, the workspace oriented optimal design of a parallel manipulator is usually the determination of parameters with respect to a desired task workspace, in which some other performances should be satisfied. This method is usually implemented by specifying the task workspace and searching the suitable parameter values using some numerical algorithm. This method has the GCI definition problem, which will be presented in the subsequent text. In this paper, our method is proposed as follows: (a) normalization of the involved design parameters and development of a design space; (b) illustration of relationships between involved performance indices and the normalized parameters graphically; (c) use of performance charts to identify the optimum region meeting kinematic performance constraints; (d) selection of a candidate from the optimum region; (e) investigation of the local performance indices of the candidate to determine the workspace, which is defined as the *good-conditioning workspace* (GCW); (f) calculation of the normalization factor by comparing the GCW and the desired task workspace; and finally, (g) determination of the parameters using the factor. Here, the normalized manipulator is defined as the *basic similarity manipulator* (BSM). All manipulators with the parameters multiplying the normalized parameters with the normalization factor are referred to as the *similarity manipulators* (SMs). The most important advantages of the design method are that the developed design space includes all possible BSMs and, due to the fact that the normalization factor doesn't change the global performance index and distribution of local index in the workspace, any one of the BSMs represents all of its SMs in terms of performances. The design method shows graphically the process how to reach the optimal result and the fact how optimal the result is.

The *local conditioning index* (LCI), which is the reciprocal of the condition number of the Jacobian matrix, has been widely utilized in the design of a parallel manipulator. The *global conditioning index* (GCI), which is the average of LCI over a workspace, was defined to evaluate the kinematic performance globally.[22] It is noteworthy that, as the average cannot describe the deviation between the maximum and minimum values of LCI, the GCI itself cannot give a full-scaled description of the overall global kinematic performance. To solve the problem, Huang et al.[23] defined a comprehensive index concerning both the mean value and range of the LCI in the task workspace. This definition was proposed with respect to the assumption that volumes of the task workspaces are the same. Another solution to this problem can be that based on the assumption that the minimum LCI values are the same but the task workspaces are different. The minimum LCI can be specified with respect to the design specification. And the set of points where the LCI values are greater than or equal to (GE) the minimum LCI is defined as the *good-conditioning workspace* (GCW). The GCI is then the average of LCI over the GCW. Therefore, if such a GCI value is bigger, we can conclude that the manipulator has a better kinematic performance in its workspace. The design method used in this paper is based on the concept that manipulators with different link lengths, the sum of which are the same, have different GCWs and different GCI values. An optimal design result can be achieved considering both the GCW and GCI. The design with respect to the stiffness criterion can be also implemented using this concept, and so others.

The basic concept of the optimal kinematic design used in this paper is the determination of the parameters of each leg length and the balance between the radii of the moving platform and the base platform with respect to desired task workspace and other related performance indices. The input limit parameters will be achieved finally. That means the input parameters are not involved in the performance analysis. As the Jacobian matrix of the studied parallel manipulator is independent of the z coordinate, the optimal kinematic design can be implemented with respect to the workspace in the $O - xy$ plane. In such a plane, the theoretical workspace is the intersection of three identical circles. There exists a *maximal inscribed circle* (MIC) in the workspace. Therefore, the task workspace of the manipulator can be a cylinder. The desired task workspace that is the design specification for an example is also given as a cylinder. The said GCW for this manipulator is actually the *good-conditioning maximal inscribed workspace* (GCMIW), which is represented by the *good-conditioning maximal inscribed circle* (GCMIC). After the normalization on the design parameters, the performance charts of the GCMIC, GCMIW-volume ratio, GCI and *global stiffness index* (GSI) are plotted. Some typical optimum regions about the normalized parameters are achieved with respect to desired performances. Such regions contain optimal candidates, from which one can pick up a suitable one according to the design condition. Given the radius of the desired task workspace, the link lengths of the design parameters can be determined by multiplying the normalized parameters with the normalization factor, which is the ratio of the radius to the GCMIC of the selected candidate. The input parameters that are needed for the manipulator to reach the task workspace can be finally achieved.

II. INVERSE KINEMATICS PROBLEM

The three translational DoFs parallel manipulator, which is an adaptation of Tsai's parallel manipulator,[13] is shown in Figure 1, where the moving platform is connected to the base by three identical serial chains, each of which is connected to the base by prismatic joint. Each of the three chains contains one parallelogram. The three parallelograms are connected to the moving platform and the sliders by revolute joints, respectively. The moving platform of the manipulator

https://doi.org/10.1017/S0263574705002079 Published online by Cambridge University Press

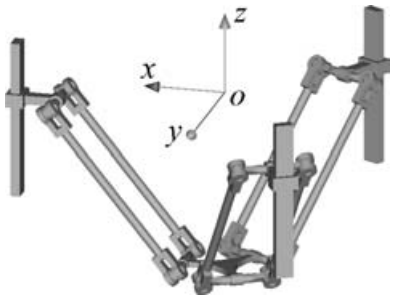

Fig. 1. Three translational DoFs parallel manipulator.

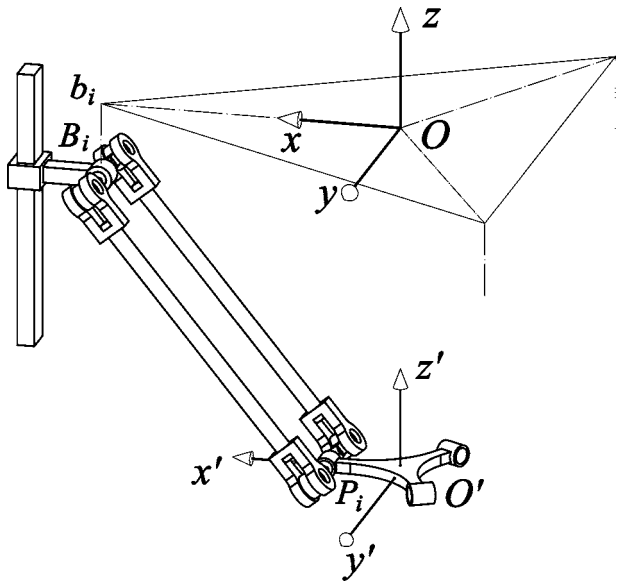

Fig. 2. Kinematic model of the manipulator with one leg.

has three translational DoFs with respect to the base. And the output can be achieved through the combination of the actuation to the three prismatic joints.

Kinematically, the studied parallel manipulator is identical with that of the Delta parallel robot with linear actuators.[8,12,14] Closed-form solutions for both the inverse and forward kinematics for the manipulator have been developed.[8] Here, for convenience, we recall the inverse kinematics problem briefly. A kinematics model of the manipulator is developed as shown in Figure 2. The center of the revolute joint that connects the parallelogram with the slider in each of the three chains is denoted as B_i $(i = 1, 2, 3)$, and the center of the revolute joint connected to the moving platform in each chain is denoted as $P_i (i = 1, 2, 3)$. A fixed global reference system $\Re : O - xyz$ is located at the center of the regular triangle $b_1b_2b_3$ with the z-axis normal to the base and the x-axis directed along Ob_1, as shown in Figure 3. Another reference system $\Re' : O' - x'y'z'$ is located at the center of the regular triangle $P_1P_2P_3$. The z'-axis is perpendicular to the output platform and x'-axis directed along $O'P_1$, as shown in Figure 3. Related geometric parameters are $Ob_i = R$, $O'P_i = r$ and $B_iP_i = R_1$, where $i = 1, 2, 3$. The objective of the inverse kinematics is to find the inputs of the manipulator with the given position of reference point O'.

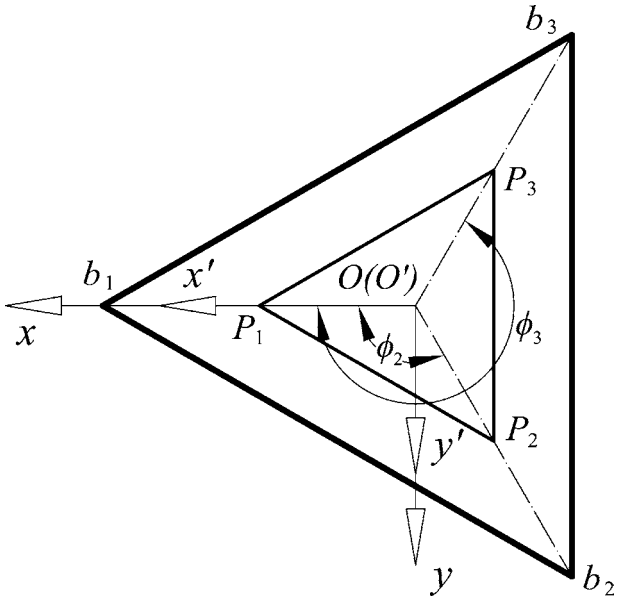

Fig. 3. Top view of the base frame and the moving platform.

The position vector $[\boldsymbol{c}]_{\Re}$ of point O' in frame $\Re$ can be written as

$$[\boldsymbol{c}]_{\Re} = (x \quad y \quad z)^{\mathrm{T}} \tag{1}$$

As shown in Figure 3, The coordinate of the point P_i in the frame $\Re'$ can be described by the vector $[\boldsymbol{P}_i]_{\Re'}$ $(i = 1, 2, 3)$, which can be expressed as

$$[\boldsymbol{P}_i]_{\Re'} = (r\cos\phi_i \quad r\sin\phi_i \quad 0)^{\mathrm{T}},\ i = 1, 2, 3 \tag{2}$$

where

$$\phi_i = \frac{2(i-1)}{3}\pi,\ (i = 1, 2, 3) \tag{3}$$

which is the angle from the x'-axis to the line $O'P_i$, as shown in Figure 3. Then vectors $[\boldsymbol{P}_i]_{\Re}$ $(i = 1, 2, 3)$ in frame $O - xyz$ can be written as

$$[\boldsymbol{P}_i]_{\Re} = (r\cos\phi_i + x \quad r\sin\phi_i + y \quad z)^{\mathrm{T}} \tag{4}$$

As shown in Figure 3, vectors $[\boldsymbol{B}_i]_{\Re}$ $(i = 1, 2, 3)$ will be defined as the position vectors of points B_i in frame $\Re$, and

$$[\boldsymbol{B}_i]_{\Re} = (R\cos\phi_i \quad R\sin\phi \quad z_i)^{\mathrm{T}},\ i = 1, 2, 3 \tag{5}$$

Then the inverse kinematics of the translational manipulator can be solved by writing following constraint equation

$$\|[\boldsymbol{P}_i - \boldsymbol{B}_i]_{\Re}\| = R_1,\ i = 1, 2, 3 \tag{6}$$

that is

$$(x - x_i)^2 + (y - y_i)^2 + (z - z_i)^2 = R_1^2 \tag{7}$$

in which, $x_i = R_2\cos\phi_i$, $y_i = R_2\sin\phi_i$, $R_2 = R - r$ and z_i are the inputs of the manipulator and can be rearranged from

https://doi.org/10.1017/S0263574705002079 Published online by Cambridge University Press

Eq. (7) as

$$z_i = \pm\sqrt{R_1^2 - (x - x_i)^2 - (y - y_i)^2} + z \tag{8}$$

from which one can see that there are eight inverse kinematics solutions for a given position of the parallel manipulator. The eight solutions correspond to eight kinds of assembly modes of the manipulator. Hence, for a given manipulator and for prescribed values of the position of the moving platform, the required actuated inputs can be directly computed from Eq. (8). The assembly configuration shown in Figure 1 corresponds to the kinematic mode that the "±" in Eq. (8) is "+".

III. JACOBIAN MATRIX AND SINGULARITY

The Jacobian matrix is defined as the matrix that maps the relationship between the velocity of the moving platform and the vector of actuated joint rates. Then we should firstly consider the velocity equation of the manipulator to obtain the Jacobian matrix. Equations (7) can be differentiated with respect to time to obtain the velocity equations, which leads to

$$(z - z_i)\dot{z}_i = (x - x_i)\dot{x} + (y - y_i)\dot{y} + (z - z_i)\dot{z},\ i = 1, 2, 3 \tag{9}$$

Rearranging Eq. (9) leads to an equation of the form

$$\boldsymbol{A}\dot{\boldsymbol{\rho}} = \boldsymbol{B}\dot{\boldsymbol{p}} \tag{10}$$

where $\dot{\boldsymbol{p}}$ is the vector of output velocities defined as

$$\dot{\boldsymbol{p}} = (\dot{x} \quad \dot{y} \quad \dot{z})^{\mathrm{T}} \tag{11}$$

and $\dot{\boldsymbol{\rho}}$ is the vector of input velocities defined as

$$\dot{\boldsymbol{\rho}} = (\dot{z}_1 \quad \dot{z}_2 \quad \dot{z}_3)^{\mathrm{T}} \tag{12}$$

In Eq. (10), $\boldsymbol{A}$ and $\boldsymbol{B}$ are, respectively, 3×3 matrices of the manipulator and can be expressed as

$$\boldsymbol{A} = \begin{bmatrix} z - z_i & 0 & 0 \\ 0 & z - z_2 & 0 \\ 0 & 0 & z - z_3 \end{bmatrix},$$
$$\boldsymbol{B} = \begin{bmatrix} x - x_1 & y - y_1 & z - z_1 \\ x - x_2 & y - y_2 & z - z_2 \\ x - x_3 & y - y_3 & z - z_3 \end{bmatrix} \tag{13}$$

If matrix $\boldsymbol{A}$ is nonsingular, the Jacobian matrix of the manipulator can be obtained as

$$\boldsymbol{J} = \boldsymbol{A}^{-1}\boldsymbol{B} = \begin{bmatrix} \dfrac{x - x_1}{z - z_1} & \dfrac{y - y_1}{z - z_1} & 1 \\ \dfrac{x - x_2}{z - z_2} & \dfrac{y - y_2}{z - z_2} & 1 \\ \dfrac{x - x_3}{z - z_3} & \dfrac{y - y_3}{z - z_3} & 1 \end{bmatrix} \tag{14}$$

For the assembly mode shown in Figure 1, the Jacobian matrix can be rewritten as

$$\boldsymbol{J} = \begin{bmatrix} \dfrac{x - R_2\cos\phi_1}{q_1} & \dfrac{y - R_2\sin\phi_1}{q_1} & 1 \\ \dfrac{x - R_2\cos\phi_2}{q_2} & \dfrac{y - R_2\sin\phi_2}{q_2} & 1 \\ \dfrac{x - R_2\cos\phi_3}{q_3} & \dfrac{y - R_2\sin\phi_3}{q_3} & 1 \end{bmatrix} \tag{15}$$

in which, $q_1 = \sqrt{R_1^2 - (x - R_2\cos\phi_i)^2 - (y - R_2\cos\phi_i)^2}$ $(i = 1, 2, 3)$.

The singularity can be achieved from Jacobian matrices $\boldsymbol{A}$ and $\boldsymbol{B}$.[24] When $|\boldsymbol{A}| = 0$ and $|\boldsymbol{B}| \neq 0$, from Eq. (13), there is $z = z_i$ $(i = 1, 2, 3)$, which means that the firs kind of singularity occurs when any one of the three legs is in a plane parallel to the $O - xy$ plane. If $|\boldsymbol{B}| = 0$ and $|\boldsymbol{A}| \neq 0$, the second kind of singularity arises. This leads to $x = x_i$ or $y = y_i$. Physically, the three legs should be parallel to each other. Then, if $R - r \neq 0$, the singularity cannot occur. $|\boldsymbol{B}| = 0$ and $|\boldsymbol{A}| = 0$ lead to the third kind of singularity. The singularity is a particular case that the three legs are all in a plane parallel to the $O - xy$ plane. Only $|R - r| = R_1$ will result in this kind of singularity.

Therefore, in order to make the manipulator be assembled and work freely, there should be $R > r$ and $R - r < R_1$ or $r > R$ and $r - R < R_1$. In this paper, we are concerned about the case that $R > r$ and $R - r < R_1$.

IV. LOCAL CONDITIONING INDEX

Mathematically, the condition number of a matrix is used in numerical analysis to estimate the error generated in the solution of a linear system of equations by the error on the data.[25] The condition number of the Jacobian matrix can be written as

$$\kappa = \|\boldsymbol{J}\|\|\boldsymbol{J}^{-1}\| \tag{16}$$

where $\|\cdot\|$ denotes the Euclidean norm of the matrix, which is defined as

$$\|\boldsymbol{J}\| = \sqrt{tr(\boldsymbol{J}^T\boldsymbol{W}\boldsymbol{J})}; \quad \boldsymbol{W} = \frac{1}{n}\mathbf{1} \tag{17}$$

in which n is the dimension of the Jacobian matrix and $\mathbf{1}$ the $n \times n$ identity matrix. Moreover, one has

$$1 \leq \kappa \leq \infty \tag{18}$$

and hence, the reciprocal of the condition number, i.e. $1/\kappa$, is always defined as the *local conditioning index* (LCI) to evalute the control accuracy, dexterity and isotropy of a manipulator.[26–29] This number is to be kept as large as possible. If the number can be unity, the matrix is an isotropic one, and the manipulator is in an isotropic configuration.

https://doi.org/10.1017/S0263574705002079 Published online by Cambridge University Press

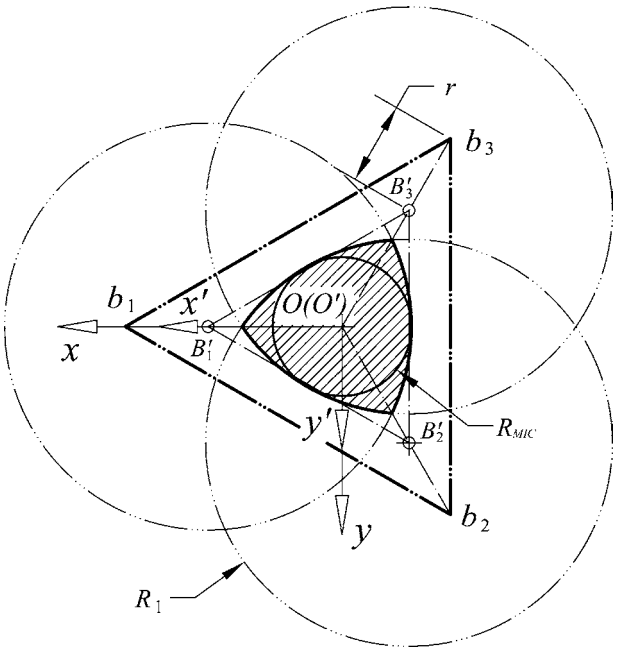

Fig. 4. The maximal workspace in the $O-xy$ plane.

V. WORKSPACE ANALYSIS

V.1. The maximal workspace in the $O-xy$ plane

Equation (15) indicates that the Jacobian matrix is independent of z value. That means the LCI $1/\kappa$ will be same if x and y are constant and whatever the z value is. As most of the performance indices are defined based on the Jacobian matrix, they also have such a characteristic on every z workspace section. Therefore, in the design process we can let z alone. To investigate the workspace performance and define global indices, we can only be concerned about the workspace at the z-section.

Disregarding the input, the maximal region that the manipulator can reach in the $O-xy$ plane is determined by the singularity, i.e. the first kind of singularity where any one of the three legs B_iP_i is parallel to the $O-xy$ plane. The maximal workspace in the $O-xy$ plane, referred to be as W_{xy} shown as the shade region in Figure 4, is actually the intersection of three circles C_i, which can be written as

$$C_i : (x-x_i)^2+(y-y_i)^2=R_1^2, \quad i=1,2,3 \tag{19}$$

If the volume of the maximal workspace is denoted as V_{W-xy}, there is

$$V_{W-xy}=3R_1^2\tan^{-1}\left[\frac{\sqrt{3}\left(\sqrt{4R_1^2-3R_2^2}-R_2\right)}{3R_2+\sqrt{4R_1^2-3R_2^2}}\right] -\frac{3\sqrt{3}}{4}R_2\left(\sqrt{4R_1^2-3R_2^2}-R_2\right) \tag{20}$$

From Figure 4, one can see that there exists a *maximal inscribed circle*[12] (MIC) within the maximal workspace W_{xy}. The MIC defines a workspace, which is referred to as the *maximal inscribed workspace* (MIW). The task workspace of the manipulator is usually a cylinder, the section of which can be the MIC. The radius of the MIC can be written as

$$R_{MIC}=R_1-R_2 \tag{21}$$

One can see that the larger the maximal workspace W_{xy}, the longer the MIC radius. Therefore, the MIC radius can be used to measure the volume size of W_{xy}.

V.2. Good-conditioning workspace in the $O-xy$ plane

As the maximal workspace W_{xy} is bounded by the singularities, one can imagine that there exist some points within the workspace where the LCI will be zero or very small. At these points, the control accuracy of the manipulator will be very poor. Practically, these points will not be used. And in the design process, they should be excluded. The left workspace that will be used in practice can be referred to as the *good-conditioning workspace* (GCW), which can be bounded by locus where the LCI is equal to a specified LCI value, i.e. $1/\kappa$. Then, the set of points where the LCI is greater than or equal to (GE) a specified LCI is defined as the GCW. As the manipulator is symmetric in structure, the distribution of some performances, e.g. LCI, should be symmetric as well. Therefore, there should exist a MIC in the GCW. Here, the MIC is defined as *good-conditioning maximal inscribed circle* (GCMIC), and the MIW bounded by such a MIC is referred to as the *good-conditioning maximal inscribed workspace* (GCMIW). Since the task workspace is usually a cylinder, the GCMIW is actually the section of the task workspace. And the optimal design of the manipulator can be implemented with respect to the GCMIW.

The LCI value indicates the distance of a point to the singularity. Figure 5 illustrates the distribution of LCI within the maximal workspace W_{xy}. It shows that the distribution is symmetry about the three lines $y=0$, $y=\sqrt{3}x$ and

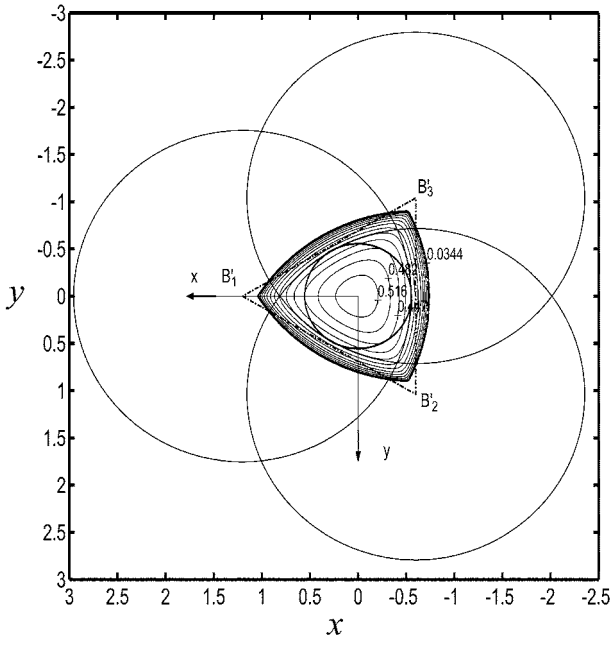

Fig. 5. Investigation of the LCI on the maximal workspace.

https://doi.org/10.1017/S0263574705002079 Published online by Cambridge University Press

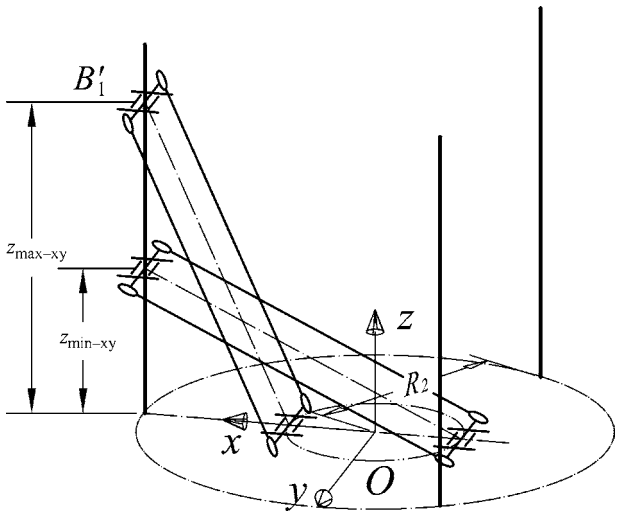

Fig. 6. Input limits of each leg within the GCMIW.

$y = -\sqrt{3}x$. On the boundary of the workspace, the LCI is zero. The nearer the distance to the origin point, the better the LCI, and at the origin point the LCI is best. It also implies that, within a circle centered at the origin point, the LCI at the three points that is nearest to the boundary of the maximal workspace W_{xy} is worst. The three points are located at the lines $y = 0$, $y = \sqrt{3}x$ and $y = -\sqrt{3}x$. Their distances to the origin point are same. The distance is, in fact, the radius of the GCMIC. Then, in order to find out a GCMIW of a given manipulator, one can search numerically the value of x within the domain $[-R_{MIC}, 0]$ using Eq. (16) with respect to a specified LCI by letting $y = 0$. If the expected x value for a specified LCI is denoted as x_{GC} ($x_{GC} \leq 0$), the GCMIC radius R_{GCMIC} can be written as

$$R_{GCMIC} = -x_{GC} \tag{22}$$

V.3. Workspace-volume ratio

The input limits of each leg can be achieved when the leg reaches its nearest and farthest points. For example, as shown in Figure 6, the input limits $z_{\max-xy}$ and $z_{\min-xy}$ for the first leg within the GCMIW can be obtained as

$$z_{\max-xy} = \sqrt{R_1^2 - (R_2 - R_{GCMIC})^2} \text{ and}$$
$$z_{\min-xy} = \sqrt{R_1^2 - (R_2 + R_{GCMIC})^2} \tag{23}$$

Thus, disregarding the workspace along z-axis, the basic volume of the manipulator can be written as

$$V_b = \pi R_2^2 z_{\max-xy} = \pi R_2^2 \sqrt{R_1^2 - (R_2 - R_{GCMIC})^2} \tag{24}$$

The GCMIW to the basic volume ratio, here, for short, *GCMIW-volume ratio*, can be expressed as

$$RA_{W-V} = \frac{R_{GCMIC}^2}{R_2^2 \sqrt{R_1^2 - (R_2 - R_{GCMIC})^2}} \tag{25}$$

VI. PERFORMANCE CHARTS OF THE GCMIC AND THE GCMIW-VOLUME RATIO

VI.1. Normalization on the geometric parameters

As well known, the performance of a parallel manipulator depends on not only the pose of the moving platform but also the link lengths (dimensions). In order to study a performance of the manipulator in detail, it is necessary to investigate the relationships between the performance evaluating index and the link lengths of the geometric parameters.

According to the analysis in section V, the Jacobian matrix $\boldsymbol{J}$, the maximal workspace W_{xy} and the GCMIW of a manipulator are heavily related to parameters R_1 and R_2. Theoretically, each of the parameters R_1 and R_2 can have any value between 0 and infinite. This is the biggest problem to study the relationship between a performance and link lengths in a finite space. For this reason, we must eliminate the physical link size of the manipulator. Let

$$D = (R_1 + R_2)/2 \tag{26}$$

which is defined as the normalization factor. One can obtain two non-dimensional parameters r_i by means of

$$r_1 = R_1/D \quad \text{and} \quad r_2 = R_2/D \tag{27}$$

Then there is

$$r_1 + r_2 = 2 \tag{28}$$

Theoretically, from Eq. (28), the two non-dimensional parameters r_1 and r_2 can have any value between 0 and 2. For the three translational DoFs parallel manipulator studied here, the analysis on the workspace and singularity shows that the two parameters should be

$$r_2 < r_1 \tag{29}$$

Considering Eq. (28) and relationship $r_2 > 0$, condition Eq. (29) can be rewritten as

$$2 > r_1 > 1 \tag{30}$$

Therefore, the normalized parameters are limited. Eq. (30) defines a design space of the manipulator. This makes it possible to show the relationship between a performance index and the geometric parameters graphically. The subsequent sections study the manipulators with non-dimensional parameters r_1 and r_2. In Eqs. (6)–(25), R_j should be replaced by r_j ($j = 1, 2$). The MIC and GCMIC radii of a normalized manipulator are accordingly denoted as r_{MIC} and r_{GCMIC}, respectively.

VI.2. Performance charts

For the non-dimensional parallel manipulators, the MIC of the maximal workspace in the $O - xy$ plane can be writes as

$$r_{MIC} = r_1 - r_2 = 2(r_1 - 1) \tag{31}$$

which is proportional to the parameter r_1.

For a given normalized manipulator with parameters r_1 and r_2, the GCMIC radius can be achieved numerically from Eq. (16) by searching the expected x value within the domain

https://doi.org/10.1017/S0263574705002079 Published online by Cambridge University Press

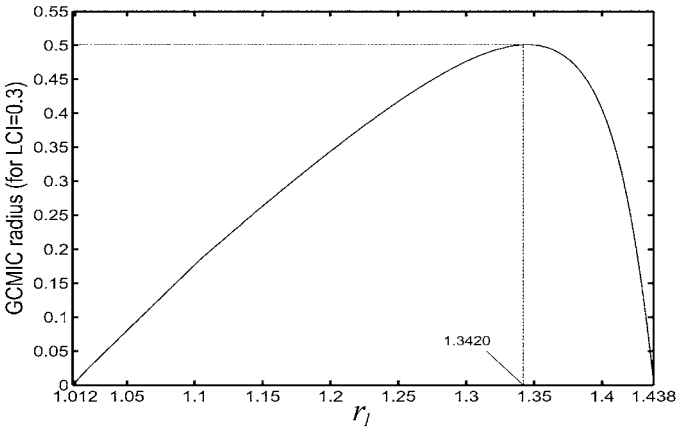

Fig. 7. Chart of the GCMIC radius when LCI is specified as 0.3.

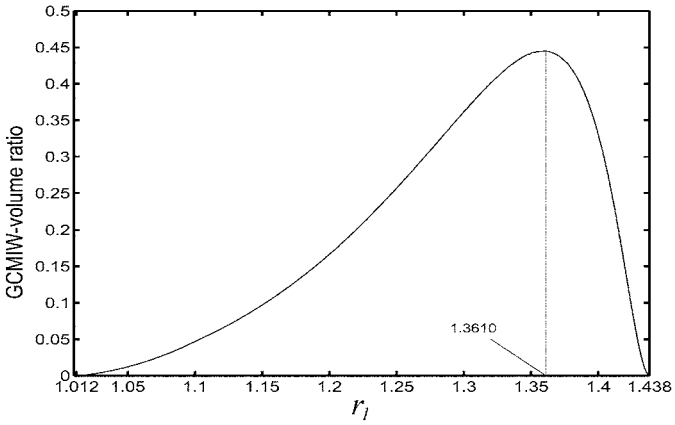

Fig. 8. Chart of the GCMIW-volume ratio when LCI is specified as 0.3.

$[-r_{MIC},\ 0]$ with respect to a specified LCI when $y = 0$. If the LCI is specified as 0.3, the relationship between the r_{GCMIC} and the normalized parameter r_1 is shown in Figure 7, from which one can see that there is the GCMIW for the normalized manipulator when $r_1 \in [1.0120, 1.4380]$, and the r_{GCMIC} reaches its maximum when $r_1 = 1.3420$.

Replacing $R_j (j = 1, 2)$ and R_{GCMIC} in Eq. (25) by r_j and r_{GCMIC}, respectively, the GCMIW-volume ratio, denoted as ra_{W-V}, of a normalized manipulator can be obtained. Figure 8 illustrates the relationship between the GCMIW-volume ratio and the normalized parameter r_1. It shows that the GCMIW-volume ratio reaches its maximum when $r_1 = 1.3610$. The comparison between Figures 7 and 8 indicates that a manipulator with longer GCMIC usually has better GCMIW-volume ratio.

VII. PERFORMANCE CHARTS OF SOME GLOBAL INDICES

As the GCW or GCMIW-volume ratio is incapable of representing the global kinematic performance in the workspace, in the optimal design of a manipulator, it cannot be the only criterion. Some other performances, such as the average of the LCI over the GCMIW and stiffness, must be involved. In this section, being as the examples, the global conditioning and stiffness indices will be investigated and presented graphically by their charts.

VII.1. Global conditioning index

The condition number κ is configuration-dependent. The LCI $1/\kappa$ is a local performance index. In section V.2, the GCW is defined with respect to a specified LCI. According to the definition, the GCW is such a region where the LCI at every point is GE the specified LCI. Therefore, one cannot be sure that a manipulator with a larger GCMIW has a better LCI average over the GCMIW, i.e. the better global behavior. In order to evaluate the global behavior of a manipulator on a workspace, a global index was defined by Gosselin and Angeles[22] as

$$\eta = \int_W 1/\kappa \, dW \Big/ \int_W dW \tag{32}$$

which is the *global conditioning index* (GCI). In Eq. (32), W is the GCMIW when LCI ≥ 0.3. In particular, a large value of the index ensures that the manipulator can be precisely controlled.

It is noteworthy that the mathematic meaning of Eq. (32) is particular. Although the GCMIWs for different manipulators are different, the minimum LCIs (0.3) are the same. Therefore, the GCI defined here can give a full-scaled description of the overall global kinematic performance to compare the performance for different manipulators, and so is the stiffness index defined in next section.

The chart of GCI for the manipulator is shown in Figure 9, from which one can see that:

- The index reaches its maximum when $r_1 = 1.1010$.
- When r_1 is less than 1.1010 and greater than 1.0120, GCI is proportional to the parameter r_1. It is inverse proportional to r_1, when r_1 is more than 1.1010 and less than 1.4380.

Comparing the chart of GCI with those of GCMIC radius and GCMIW-volume ratio, it is not difficult to find out that a manipulator with larger GCMIW or better GCMIW-volume ratio usually has worse GCI, and a manipulator with better GCI usually has smaller GCMIW or worse GCMIW-volume ratio.

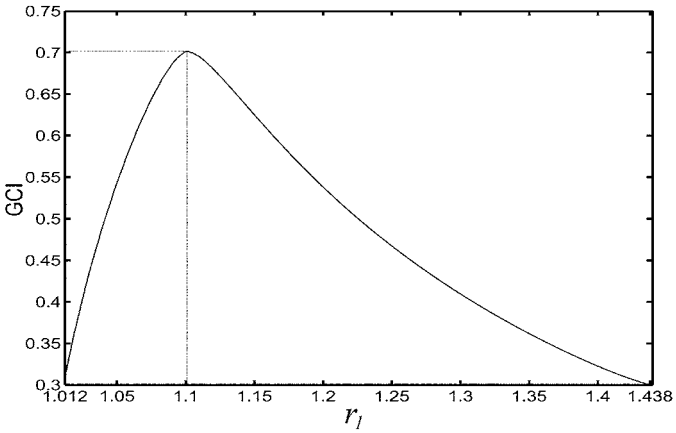

Fig. 9. Chart of the GCI with respect to the GCMIW when LCI is specified as 0.3.

https://doi.org/10.1017/S0263574705002079 Published online by Cambridge University Press

VII.2. Global stiffness index (GSI)

There will be deformation on the end-effector if the external force acts on it. The deformation is depended on the manipulator stiffness and the external force. The manipulator stiffness affects the dynamics and the position accuracy of the device, for which stiffness is an important performance index. Especially, the static stiffness (or rigidity) of the manipulator can be a primary consideration in the design of a parallel manipulator for certain applications, e.g., machine tools.

In the operational coordinate space, we define a stiffness matrix $\boldsymbol{K}$ that relates the external force vector $\boldsymbol{\tau}$ at the moving platform to the output displacement vector $\boldsymbol{D}$ of the moving platform according to

$$\boldsymbol{D} = \boldsymbol{K}^{-1}\boldsymbol{\tau} \tag{33}$$

where the stiffness matrix $\boldsymbol{K}$ is expressed as

$$\boldsymbol{K} = \boldsymbol{J}^{T}\boldsymbol{K}_{p}\boldsymbol{J} \tag{34}$$

with

$$\boldsymbol{K}_{p} = \begin{bmatrix} k_{p1} & \\ & k_{p2} \end{bmatrix} \tag{35}$$

in which k_{pi} is a scalar representing the stiffness of each of the actuators.

If $k_{p1} = k_{p2} = 1$ and $\|\boldsymbol{\tau}\|^2 = 1$, by establishing the Lagrange equation,[20] the maximum and minimum deformations can be obtained as

$$\|\boldsymbol{D}_{\max}\| = \sqrt{\max(|\lambda_{Di}|)} \text{ and } \|\boldsymbol{D}_{\min}\| = \sqrt{\min(|\lambda_{Di}|)} \tag{36}$$

where λ_{Di} $(i = 1, 2)$ are the eigenvalues of the matrix $(\boldsymbol{K}^{-1})^{\mathrm{T}}\boldsymbol{K}^{-1}$. $\|\boldsymbol{D}_{\max}\|$ and $\|\boldsymbol{D}_{\min}\|$ are actually the maximum and minimum deformations on the end-effector when both the external force vector and the matrix $\boldsymbol{K}_p$ are unity. The maximum and minimum deformations form a deformation ellipsoid, whose axes lie in the directions of the eigenvectors of the matrix $(\boldsymbol{K}^{-1})^{\mathrm{T}}\boldsymbol{K}^{-1}$. Its magnitudes are the maximum and minimum deformations given by Eq. (36). Usually, the deformation $\|\boldsymbol{D}_{\max}\|$ can be used to evaluate the stiffness of a manipulator, which is defined as the *local stiffness index* (LSI). The smaller the deformations, the better the stiffness.

Similarly, based on Eq. (36), the *global stiffness index* (GSI) that can evaluate the stiffness of a manipulator within the workspace is defined as

$$\eta_D = \frac{\int_W \|\boldsymbol{D}_{\max}\| dW}{\int_W dW} \tag{37}$$

where, for the manipulator studied here, W is the GCMIW when LCI ≥ 0.3. Usually, η_D can be used as the criterion to design the manipulator with respect to the stiffness. Normally, we expect that the index value should be as small as possible.

Figure 10 shows the relationship between the GSI η_D and the normalized parameter r_1. The chart indicates that η_D is proportional to r_1, i.e. the global stiffness of a manipulator is inverse proportional to r_1.

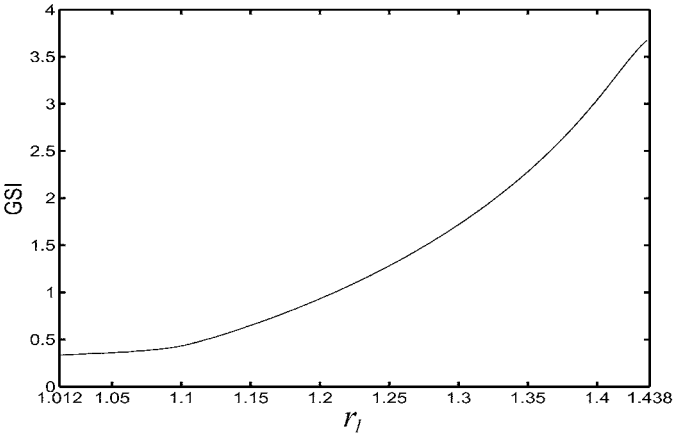

Fig. 10. Chart of the GSI with respect to the GCMIW when LCI is specified as 0.3.

VIII. OPTIMUM DESIGN EXAMPLE BASED ON THE CHARTS

VIII.1. Optimum region with respect to desired performances

In the last sections, the parameters of the three translational DoFs parallel manipulator were normalized. The normalization makes it possible to illustrate the relationship between a performance index and the normalized parameters in a limited space. And the indices for workspace, control accuracy (isotropy, dexterity), and stiffness of the manipulator have been studied and corresponding performance charts have been plotted. These charts can be used in the optimum design of the manipulator in this section.

Here, the optimum region with non-dimensional parameter with respect to desired performances will be first given.

VIII.1.1. GCMIW-volume ratio and GCI. In almost all designs, the workspace and GCI are usually considered. In terms of the workspace performance, a high GCMIW-volume ratio is always welcome. At the same time, a good GCI performance within the workspace is preferred. From Figure 8, we can see that, within the region $r_1 \in [1.0120,\ 1.4380]$, the relationship between the GCMIW-volume ratio and the parameter r_1 is non-monotone, and so is that between GCI and the parameter. Therefore, it is impossible to find a manipulator with best GCI and, at the same time, highest GCMIW-volume ratio. This is also the universal problem in the issue of optimum design, especially, with multi-performances. Undoubtedly, in some applications, if it is not necessary to care about the GCI but only the GCMIW-volume ratio, the designer can select candidates near $r_1 = 1.3610$. Similarly, if the designer is just concerned about the GCI and let the GCMIW-volume ratio alone, he can pick up an optimal candidate near $r_1 = 1.1010$. But, for the problem considered here, if the GCMIW-volume ratio is specified as $ra_{W-V} \geq 0.2$ and GCI $\eta \geq 0.45$, we can obtain a common

https://doi.org/10.1017/S0263574705002079 Published online by Cambridge University Press

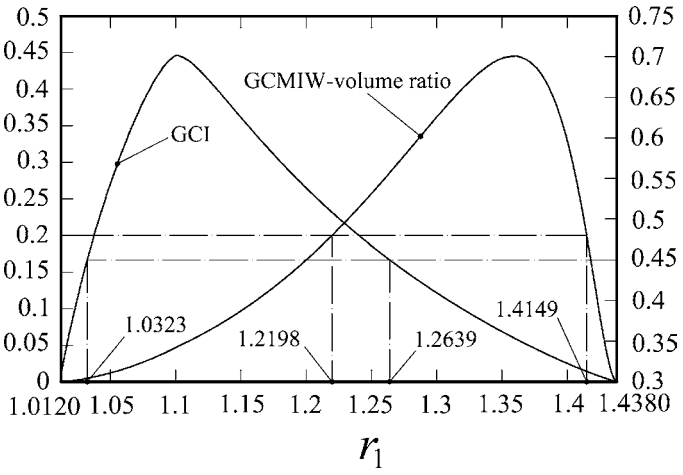

Fig. 11. One optimum region with desired ra_{W-V} and GCI.

region $\Omega_{RA\text{-}GCI} = [r_1 | 1.2198 \le r_1 \le 1.2639]$, as shown in Figure 11, subjected to both of the specifications. Such a region can be one optimum design region if both GCMIW-volume ratio and GCI performances are considered. This region gives the possible geometric parameters r_1 and r_2 ($r_2 = 2 - r_1$) of the manipulator, which has desired GCMIW-volume ratio and GCI performances. For example, the manipulator with $r_1 = 1.23$ and $r_2 = 0.77$ can be one candidate of the optimum design. The two performance indices are $ra_{W-V} = 0.2185$ and $\eta = 0.4939$, respectively. And its GCMIC radius is $r_{GCMIC} = 0.3893$ when LCI ≥ 0.3.

VIII.1.2. GCMIW-volume ratio, GCI and GSI. In this paper, the stiffness is evaluated by the maximum deformation of the end-effector when the external force and the stiffness of each of the actuators are unit. Taking into account the stiffness, usually, we expect the index η_D to be as small as possible. To achieve an optimum region with respect to the three indices, the GCMIW-volume ratio can be specified as $ra_{W-V} \ge 0.2$, GCI $\eta \ge 0.45$ and GSI $\eta_D \le 1.3$. The optimum region will be $\Omega_{RA\text{-}GCI\text{-}GSI} = [r_1 | 1.2198 \le r_1 \le 1.2523]$. For example, the evaluating criterion of the GSI of the manipulator with parameters $r_1 = 1.23$ and $r_2 = 0.77$ is $\eta_D = 1.1333$.

VIII.1.3. GCI and GSI. In the micro application where large workspace is not needed, the GCI and GSI can be considered only. Figure 10 shows that a shorter r_1 will lead to better stiffness performance. Comparing Figures 9 and 10, one can find out that a manipulator with better GCI usually has higher stiffness. For instance, the manipulator in the region $\Omega_{GCI\text{-}GSI} = [r_1 | 1.0769 \le r_1 \le 1.1180]$ has very good GCI and stiffness performances. For example, the GCI and GSI the manipulator with parameters $r_1 = 1.1$ and $r_2 = 0.9$ are $\eta = 0.7006$ and $\eta_D = 0.4323$, respectively.

VIII.2. Dimension determination based on the obtained optimum example with respect to a desired task workspace

The final objective of optimum design is to determine the link lengths of a manipulator. In the last section, some optimum regions have been presented as examples. These regions consist of manipulators with non-dimensional parameters. The selected optimum manipulators with non-dimension are comparative results. They are not the final results. In this section, the dimension of an optimal manipulator will be determined with respect to a desired task workspace.

As an example to present how to determine the dimensional parameters of a non-dimensional optimum manipulator achieved in section VIII.1. we consider the manipulator with $r_1 = 1.23$ and $r_2 = 0.77$ selected in section VIII.1.2. The manipulator is from the optimum region $\Omega_{W\text{-}GCI\text{-}GSI}$, where the workspace, GCI and stiffness are involved in the design objective.

Supposing that the desired task workspace of a three translational DoFs parallel manipulator is a cylinder with $\phi 30\,\text{mm} \times 20\,\text{mm}$, the process to reach the dimension with respect to the workspace can be summarized as following:

Step 1: Investigating the distribution of LCI and LSI in the GCMIW. For the aforementioned example, the distribution is shown in Figure 12 (a) and (b), respectively, from which one can see that the LCI reaches it's maximum at the origin point ($x = 0,\ y = 0$), where the stiffness is also best.

Step 2: Determining the normalization factor D, which was used to change the dimensional geometric parameters of a manipulator to those with non-dimension. From Eq. (21), we can see that the MIC of a manipulator with parameters R_j ($j = 1, 2$) is D-time that of its normalized manipulator with parameters r_j. As the normalization factor D cannot change the Jacobian matrix $\boldsymbol{J}$ (check Eq. (15)), it cannot result the LCI in different as well. Therefore, the GCMIC of the manipulator with R_j must be D-time that of its normalized manipulator, i.e.,

$$R_{GCMIC} = D r_{GCMIC} \tag{38}$$

Once the GCMIC radius of a normalized manipulator is determined, the normalization factor D can be achieved using Eq. (38). For example, if the investigation on the LCI and LSI is available, the GCMIC of the example remains 0.3893. Based on Eq. (38), the factor D can be obtained as $D = 15 \big/ 0.3893 \approx 38.5307\,\text{mm}$.

Step 3: Achieving the dimensional parameters of the optimum manipulator using the normalization factor D. As given in Eq. (27), the relationship between a dimensional parameter and a non-dimensional one is $R_j = D r_j$. Then, if D is determined, R_i can be achieved accordingly. For the above example, there are $R_1 \approx 47.40\,\text{mm}$ and $R_2 \approx 29.67\,\text{mm}$.

The investigation in **Step 1** shows that the stiffness at points ($x = -15,\ y = 0$) and its two symmetric points is worst. Therefore, the stiffness at the point of the designed manipulator should be checked. Note that in the definition of the LSI, the stiffness of each of the actuators and the norm of the external force vector are both supposed to be unit. In this step, one should use the real stiffness of each actuator and the external force in the application to check the stiffness at the stiffness worst point. The examination determines whether it should adjust the GCMIC radius r_{GCMIC} or not. For example, if the stiffness at the stiffness worst points and their neighborhoods cannot satisfy the specification on stiffness, one can increase the specified LCI value to decrease the GCMIC radius. In contrary, if the stiffness and control accuracy are allowed, one can decrease the specified LCI

https://doi.org/10.1017/S0263574705002079 Published online by Cambridge University Press

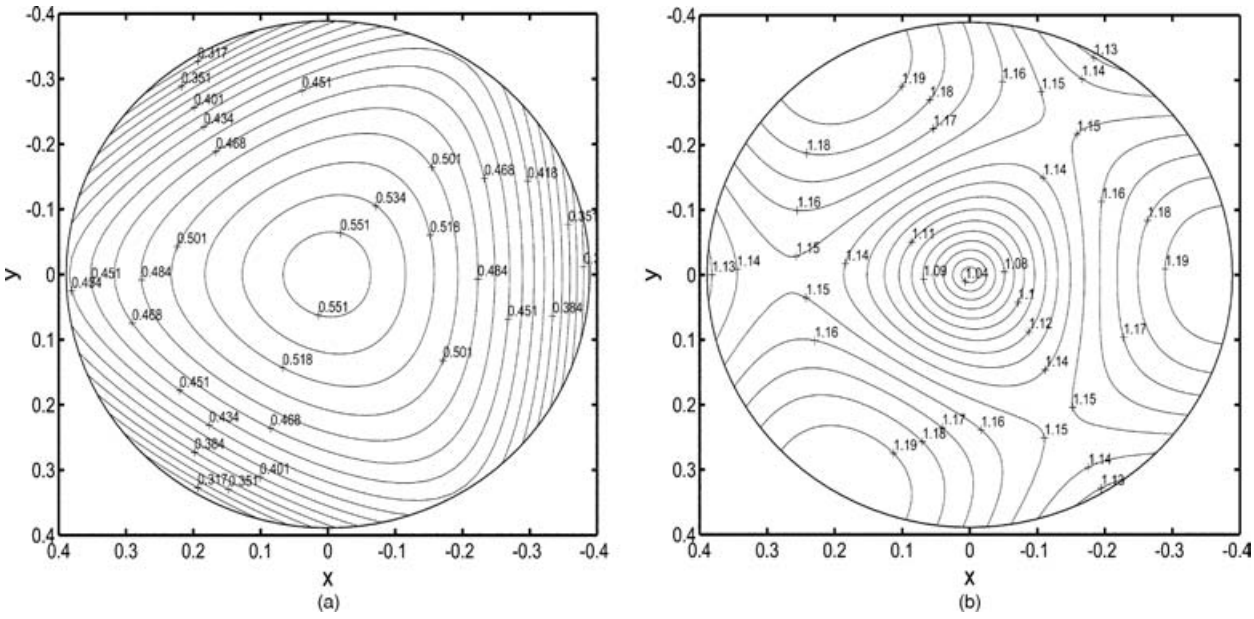

Fig. 12. Distribution of the LCI and LSI in the GCMIW of the non-dimensional manipulator: (a) LCI; (b) LSI.

value to increase the GCMIC radius. If the GCMIC radius r_{GCMIC} should be adjusted, calculate its new value using Eq. (16) by changing the specified LCI value and jump to **Step 2,** otherwise, go to **Step 4**.

Step 4: Calculating the input limit for each actuator. If we put the bottom section of the cylinder workspace on the $O-xy$ plane, the input limits of the designed manipulator can be written as

$$z_{\max} = z_{\max-xy} + H \quad \text{and} \quad z_{\min} = z_{\min-xy} \tag{39}$$

where, H is the height of the cylinder workspace and $z_{\max-xy}$ and $z_{\min-xy}$ can be achieved from Eq. (23), in which the R_{GCMIC} is actually the radius of the cylinder workspace. For the example, if it is not necessary to adjust the GCMIC radius r_{GCMIC} in Step 3, there are $z_{\max} = 65.0727$ mm and $z_{\min} = 15.8541$ mm for the design manipulator.

For the manipulator studied here, the final objective of the optimal kinematic design is the determination of parameters R_1, $R - r = R_2$ and the input limits $z_{\max}$ and $z_{\min}$. By now, the parameters are all achieved. Practically, we are concerned about the parameters R and r but not R_2 itself. Actually, the determination of r depends on the practical design of the device. As we cannot predict any design condition, this is not the content of the paper. As an example, letting $r = 12$ mm, the parameters of the designed manipulator are $R_1 = 47.40$ mm, $R = 41.67$ mm, $r = 12$ mm, $z_{\max} = 65.0727$ mm and $z_{\min} = 15.8541$ mm.

IX. SIMILARITY MANIPULATORS

In the proposed design method described in section VIII, we take it for granted that the designed manipulator is optimal if its normalized manipulator is optimal. Why? Firstly, let's check the performances of the designed manipulator. Figure 13 (a) shows the distribution of LCI in the z-section of the desired task workspace, from which one can see that the distribution is the same as that shown in Figure 12 (a) of the normalized manipulator. The GCI is still equal to 0.4939. Figure 13 (b) illustrates the distribution of LSI in the workspace section. Comparing Figure 13 (b) with Figure 12 (b), it is not hard to see that the distributions of LSI are the same as well. What is more, quantitatively, the GSI value is also 1.1333. Then, the factor D doesn't change the GCI and GSI and the distributions of LCI and LSI in the workspaces. For such reasons, all manipulators with parameters $R_j = Dr_j$ are defined as the *similarity manipulators* (SMs). The normalized manipulator with parameters r_j are referred to as the *basic similarity manipulator* (BSM). Thus, all SMs are similar in terms of performances. As the parameters of any one of the SMs can be expressed by those of the BSM, the BSM stands for not only itself but also all of its SMs in terms of performances. All BSMs are embodied in a limited design space. The optimal normalized manipulator, which is one of the BSMs in the design space, is from the optimum region, which is the intersection considering desired criteria. We can conclude that the designed manipulator that is one of its SMs is also optimal.

X. CONCLUSION

This paper proposes an optimal kinematic design method to determine the geometric parameters of a three translational DoFs parallel manipulator. The key issue of this design method is to establish a geometric design space based on the involved geometric parameters, which can embody all *basic similarity manipulators*. Then, performance charts of desired indices can be plotted. These charts can be used to identify an optimal region, from which an ideal candidate can be selected. The real-dimensional parameters can be achieved by comparing the desired task workspace and the *good-conditioning maximal inscribed workspace* of the *basic similarity manipulators*. Compared with other design

https://doi.org/10.1017/S0263574705002079 Published online by Cambridge University Press

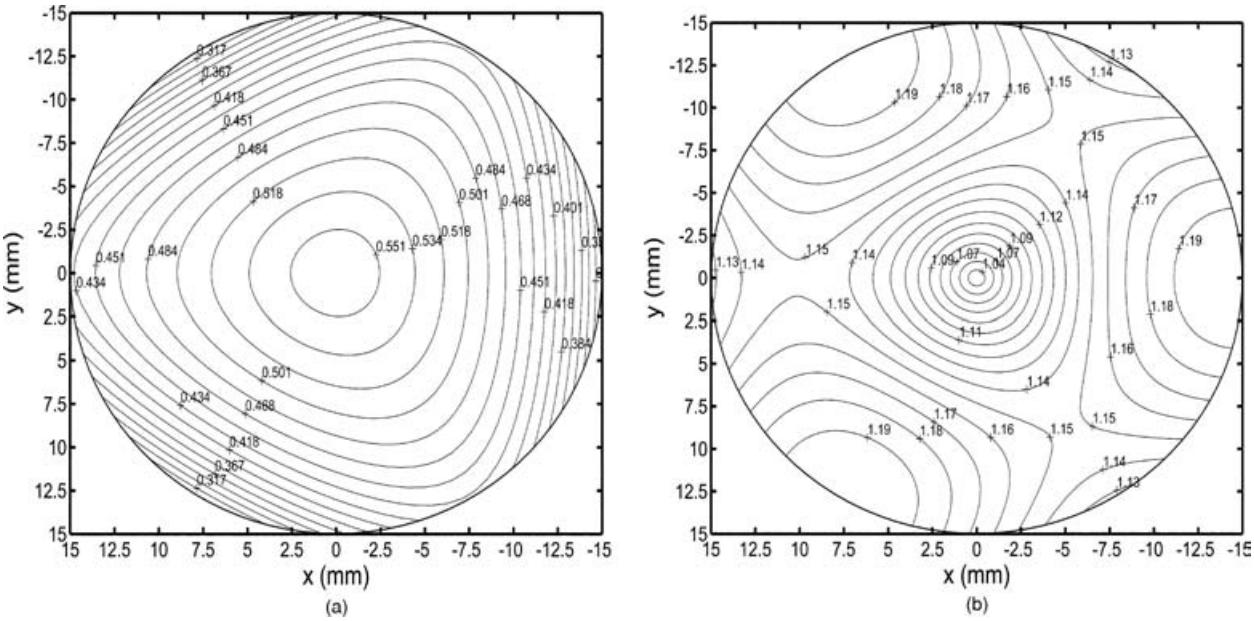

Fig. 13. Distribution of the LCI and LSI in the workspace section along z-axis of the designed manipulator: (a) LCI; (b) LSI.

methods, the proposed methodology has some advantages as follows: (a) one performance criterion corresponds to one chart, which can graphically and globally show the relationship between the criterion and design parameters; (b) for such a reason in (a), the fact that some performance criteria are antagonistic is no longer a problem in the design; (c) the optimum design process can consider multi-objective functions or multi-criteria, and also guarantees the optimal result; and finally, (d) as the optimum design can be carried out by using performance charts, this methodology shall be said to be acceptable in practice.

References

1. R. Clavel, "DELTA: a fast robot with parallel geometry," *18th Int. Symp. on Industrial Robot* (1988) pp. 91–100.
2. R. Clavel, "Device for displacing and positioning an element in space," *WIPO Patent*, WO 87/03528 (1986).
3. F. Sternheim, "Tridimensional computer simulation of a parallel robot, result for the 'DELTA4' machine," *Proc. Int. Symposium on Industrial Robots*, Lausanne (1988) pp. 333–340.
4. F. Pierrot, C. Reynaud and A. Fournier, "DELTA: a simple and efficient parallel robot," *Robotica* **8**, Part I, 105–109 (1990).
5. A. Codourey, "Dynamic modelling and mass matrix evaluation of the DELTA robot for axes decoupling control," *Proceedings of IEEE IROS'96* (1996) pp. 1211–1218.
6. M.-O. Demaurex, "The Delta robot within the industry," In: (C. R. Boer, L. Molinari-Tosatti and K. S. Smith; editors), *Parallel Kinematic Machines* (Springer-Verlag London 1999) pp. 395–399.
7. F. Holy and K. Steiner, "Machining system with movable tool head," *US Patent*: 6161992 (2000).
8. O. Company and F. Pierrot, "Modelling and preliminary design issues of a 3-axis parallel machine-tool," *Mechanism and Machine Theory* **37**, 1325–1345 (2002).
9. D. Chablat and Ph. Wenger, "Architecture optimization of a 3-DoF parallel mechanism for machining applications: the Orthoglide," *IEEE Transactions on Robotics and Automation* **19**, No. 3, 403–410 (2003).
10. X.-J. Liu, J. Jeong and J. Kim, "A three translational DoFs parallel cube-manipulator," *Robotica*, **21** Part 6, 645–653 (2003).
11. X.-J. Liu, J. Wang and H. Zheng, "Workspace atlases for the computer-aided design of the Delta robot," *Proceedings of the I. MECH. E. Part C: Journal of Mechanical Engineering Science* **217**, 861–869 (2003).
12. X.-J. Liu, J. Wang, K.-K. Oh and J. Kim, "A new approach to the design of a DELTA robot with a desired workspace," *Journal of Intelligent & Robotic Systems* **39**, No. 2, 209–225 (2004).
13. L. W. Tsai and R. Stamper, "A parallel manipulator with only translational degrees of freedom," *ASME 1996 Design Engineering Technical Conference*, Irvine, CA (1996) 96-DETC-MECH –1152.
14. D. Chablat, Ph. Wenger, F. Majou and J.-P. Merlet, "An interval analysis based study for the design and the comparison of three-degrees-of-freedom parallel kinematic machines," *Int. J. Robotics Research* **23**, No. 6, 615–624 (2004).
15. A. Kosinska, M. Galicki and K. Kedzior, "Determination of parameters of 3-dof spatial orientation manipulators for a specified workspace," *Robotica*, **20**, Part 2, 179–183 (2002).
16. E. Ottaviano and M. Ceccarelli, "Optimal design of CaPaMan (Cassino Parallel Manipulator) with a specified orientation workspace," *Robotica*, **20**, Part 2, 159–166 (2002).
17. R. E. Stamper, L.-W. Tsai and G. C. Walsh, "Optimization of a three DOF translational platform for well-conditioned workspace,"*Proceedings of IEEE International Conference on Robotics and Automation*, New Mexico (1997), pp. 3250–3255.
18. J. Ryu and J. Cha, "Volumetric error analysis and architecture optimization for accuracy of HexaSlide type parallel manipulators," *Mechanism and Machine Theory* **38**, 227–240 (2003).
19. J. J. Cervantes-Sánchez, J. C. Hernández-Rodríguez and J. Angeles, "On the kinematic design of the 5R planar, symmetric manipulator," *Mechanism and Machine Theory* **36**, 1301–1313 (2001).
20. X.-J. Liu, "The relationships between the performance criteria and link lengths of the parallel manipulators and their design theory," *Ph.D thesis* (Yanshan University, Qinhuangdao, China, 1999).
21. X.-J. Liu, J. Wang and F. Gao, "Performance atlases of the workspace for planar 3-DOF parallel manipulators," *Robotica* **18**, No. 5, 563–568 (2000).
22. C. Gosselin and J. Angeles, "A global performance index for the kinematic optimization of robotic manipulators,"

https://doi.org/10.1017/S0263574705002079 Published online by Cambridge University Press

Transaction of the ASME, Journal of Mechanical Design **113**, 220–226 (1991).
23. T. Huang, et al., "Conceptual design and dimensional synthesis of a novel 2-DOF translational parallel robot for pick-and-place operations," *Journal of Mechanical Design* **126**, 449–455 (2004).
24. H. R. M. Daniali, P. J. Zsombor-Murray, and J. Angeles, "Singularity analysis of a general class of planar parallel manipulators," *Proceedings of IEEE International Conference on Robotics and Automation*, Nagoya, Japan (1995) pp. 1547–1552.
25. G. Strang, *Linear Algebra and its Application* (Academic Press, New York, 1976).
26. J. K. Salisbury and J. J. Craig, "Articulated hands: force control and kinematic issues," *Int. J. Robot. Res.* **1**, No.1, 4–12 (1982).
27. C. A. Klein and B. E. Blaho, "Dexterity measures for the design and control of kinematiclly redundant manipulators," *Int. J. Robotics Research* **6**, No. 2, 72–82 (1987).
28. J. Angeles and C. Lopez-Cajun, "The dexterity index of serial-type robotic manipulators," *ASME Trends and Developments in Mechanisms, Machines and Robotics* 79–84 (1988).
29. C. M. Gosselin and J. Angeles, "The optimum kinematic design of a spherical three degree-of-freedom parallel manipulator," *J. Mech. Transm. Autom. Des.* **111**, 202–207 (1989).

https://doi.org/10.1017/S0263574705002079 Published online by Cambridge University Press